IEEE Access
Multidisciplinary ⋮ Rapid Review ⋮ Open Access Journal

Received 12 February 2022, accepted 22 March 2022, date of publication 19 April 2022, date of current version 6 January 2023.

Digital Object Identifier 10.1109/ACCESS.2022.3166816

Trajectory Tracking Strategy for Sliding Mode Control With Double Closed-Loop for Lawn Mowing Robot Based on ESO

LEPENG SONG, (Fellow, IEEE), JINPEN HUANG, QIN LIANG, LING NIE, XIANWEN LIANG, AND JIANQU ZHU

School of Electrical Engineering, Chongqing University of Science and Technology, Chongqing 401331, China

Corresponding author: Ling Nie (ck20220204@126.com)

This work was supported in part by the Natural Science Foundation of Chongqing under Grant cstc2018jcyjAX0336; in part by the Science and Technology Research Program of Chongqing Municipal Education Commission under Grant KJQN201801516, Grant KJQN201901536, and Grant KJQN202001531; and in part by the Graduate Innovation Program of Chongqing University of Science and Technology under Grant YKJCX1920401, Grant YKJCX1920414, and Grant YKJCX2020403.

ABSTRACT The mowing robots work with a multivariable strong coupling underactuated system that is mostly troubled by difficulty controlling and unsatisfactory accuracy. Especially, the frequent external disturbances and parameter changes are likely to get missed and heavy cutting. In this paper, a new trajectory tracking control method based on extended state observer (ESO) is introduced with a particular focus on dual closed-loop sliding mode. Firstly, from the perspective of kinematics, a speed assistant controller was designed to generate the speed control quantity, and secondly, a sliding mode control algorithm based on the improved Fractional Power Rate Reaching Law (IFPRRL) was programmed to control the drive motor that tracked the speed control quantity. By means of comparison, our improved algorithm presented faster arrival time and better robustness along with similar jittering. At the same time, the robustness of the system was further enhanced with the help of an optimized ESO to tackle unmodeled disturbances and uncertain disturbances during the operation. Finally, the experimental analysis of the motor drive circuit and the trajectory tracking control system of the lawn mowing robot were both carried out respectively. The analysis shows that the performance of the proposed reaching law sliding mode control algorithm had some new pleasing changes, such as adjustment time and robustness. The circular trajectory and the detour mowing trajectory were respectively tracked in the double closed-loop sliding mode designed in this paper. The experimental goal was to ensure that the error vector $P_e = (x$ Axis position error x_e, y Axis position error y_e, Angle error $\theta_e)$ all remaining at (0.01m, 0.01m, 0.01rad) were 5.34s and 5.36s, respectively, and both could be finally converged to 0. The results show that the newly developed controller based on ESO presented smaller arrival time and stronger robustness. The dual-closed-loop control of sliding-mode trajectory tracking method was capable to meet the real-time and precision requirements of the lawnmower robot for quick trajectory tracking.

INDEX TERMS Sliding mode control, mowing grass robot, fractional power rate reaching law, extended state observer, trajectory tracking.

I. INTRODUCTION

As a basic crop for urban greening and garden decoration, lawns are widely planted in parks, golf courses, private houses and other places. Beautiful and tidy lawns give people a feeling of refreshment. High-quality lawns therefore require a lot of manpower and material resources to maintain, especially the pruning job involving a complicated process and high cost. In order to achieve the purpose of reducing manpower and cost, more and more countries began to use lawn robots to take over the mowing job. Thanks to decades of development, the relevant technical level has made progress that is quite impressive [1]. Nonetheless, the working process of the lawn mower robot may have its mowing trajectory deviated due to the changeable terrain and intricate obstacles, leading to such misoperation as missing and re-cutting in

The associate editor coordinating the review of this manuscript and approving it for publication was Shihong Ding.

some areas. This gave birth to a higher requirement for real-time planning of the mowing path, for accurate path tracking is the key to achieve full coverage of the mowing area with no deviation. Targeting the trajectory tracking of the lawn mower robot, industry professionals have achieved initial results from their in-depth research. In this work, the path tracking mechanism was investigated as to the lawn mower robot with a three-wheel differential drive.

At present, the trajectory tracking control methods of three-wheel differential drive robots are commonly involved with PID control [2]–[4], back-stepping [5]–[7], and intelligent control [8]–[11] as well as adaptive control [12]–[16] and sliding mode variable structure control [17]–[21], etc. As a simple and reliable working mode, PID control is widely applied in tracking the trajectory of mobile robots. Victor Julio E. Normey-Rico *et al.* created a PID path tracking controller based on the kinematics model, and verified the feasibility of the PID controller on differentially driven mobile robots [2]. Literature [3] determined the PID controller parameters according to the minimum root mean square error (RMSE) of the rotational deviation of each wheel, proving that PID may have certain tracking advantages. Note that when it encounters the complex system of non-linear, underactuated and strong coupling such as lawn mowing robot, it may not be able to perform well in real-time and robustness [22]. Inversion control is a design method of forward-backward recursion, suitable for online control, real-time performance. Literature [5]–[7] studied the trajectory tracking problem of mobile robots under different conditions, introducing a back-stepping control concept. The simulation results showed that it performed well in a static environment, but held back by each simulation being allowed to only solve for a fixed time, not that much satisfactory as to the performance of the nonlinear system. The neural networks features amazing learning ability and has somehow been witnessed in the field of tracking control of wheeled mobile robots. Literature [8] worked with artificial neural network (ANN) to provide a strict trajectory tracking control method. Literature [9] proposed a kind of special tracking control strategy based on a three-layer neural network, which cleared up tracking problem by way of the Learning by Demonstration (LFD). In addition to using data learning and demonstration learning, Literature [10] also suggested a vision-based tracking model, which is a typical vision method for robot tracking associated with wavelet decomposition and artificial neural network (WD-ANN), which helped implement model building and trajectory tracking. Although the intelligent control function represented by neural network is powerful, the engineering application is far from being reliable, scalable, and maintainable due to the complex calculation and high hardware requirements. The wheel-style mobile robot is required to adapt to the complex and changeable working environment, so its mathematical model is difficult to establish accurately, which may bring many uncertain factors to the accurate control of the system. The study of adaptive control is aimed at systems with a certain degree of uncertainty, so some scholars tend to use of adaptive control algorithms in trajectory tracking control. Martins *et al.* developed an adaptive controller, which enabled the parameters of the robot dynamics to be updated online, so that the system worked with smaller errors and better performance [12] Literature [13] explored uncertain nonholonomic tracking of mobile robot paths. Combined with the actuator dynamics, a simple adaptive control method was established by the use of adaptive control techniques to handle all uncertainties with good results. Literature [14] successfully constructed an adaptive robust tracking controller, which could offset the parameter uncertainty in a wheeled mobile robot asymptotically and accurately. The research of the Literature [15] was connected with a new scheme of adaptive virtual speed controller and torque control law. To obtain the feedforward compensation, disturbance observers were placed for estimating lumped disturbances. The adaptive control method can well solve the uncertain disturbance, but through a hard process due to the cumbersome design, high cost and complex realization.

The variable structure control is nonlinear and was proposed by the former Soviet Union scholars Emelyanov and Utkin [23] since 1950s, and has developed into a relatively independent research branch. This is a non-fixed system structure that may change regularly with the current state of the system, forming a unique ''sliding mode'' that moves along the state trajectory. Therefore, it is also called Sliding Mode Control (SMC). Because the ''sliding mode'' can be created by itself and need no more job from system parameters and disturbances, it is quite impressive for simple design, fast response and strong robustness. It is worth noting that after the state reaches the sliding surface, it would be difficult to ensure that it could stay on the sliding surface rather than travel back and forth, resulting in jittering. This is unbearable for general controller actuators. That's why how to reduce the jittering is vital in sliding mode control, hence coming into the vision of peers.

Commonly used methods for suppressing jittering may cover boundary layer [24]–[26], filtering mode [27], [28], high-order sliding mode control [29]–[35] or reaching law [36]–[40], etc. The boundary layer method involves the use of a saturation function instead of a switching function, which may effectively suppress jittering, yet at the expense of system robustness. The filtering mode is proven to be effective on smoothly filtering the control signal and eliminating jittering. Unfortunately, the credits are reduced because of difficulties in maintaining the post-filtering stability of the system, making the process of stability analysis more complicated. The high-order sliding mode can not only effectively suppress output jittering, but also ensure good robustness, especially in some high-order nonlinear systems. This feature comes along at the cost of the complexity of the closed-loop system and should be used with caution due to design complexity [32]. The reaching lawology was proposed by Gao and Hung [36], who worked out three commonly used ways: index reaching law, isokinetic reaching law, and sub-order reaching law. This method can subtly adjust the

reaching law parameters to reduce high-frequency buffeting under the premise of ensuring the dynamic quality of the system, thus drawing a lot of eyeballs from peers. For example, Literature [37] discussed an Exponential Reaching Law (ERL) method, used an exponential function that dynamically adapted to changes in the controlled system to design a nonlinear approach law. Control input jittering was reduced while maintaining the high tracking performance of the controller in steady state. Literature [38] improved ERL and recommended an Enhanced Exponential Reaching Law (EERL), which had been successfully applied to wind power generation systems. Reference [39] introduced a Power Rate Exponential Reaching Law (PRERL) reaching law to improve controller arrival time and reduce jittering. Reference [40] set its focus on a Fractional Power Rate Reaching Law (FPRRL), which was an improved version in terms of arrival time, robustness, and reduced jitter when compared to the conventional reaching law. The reaching law is regarded as a good control scheme, characterized by a simple design and control dynamics.

To sum up, accurately tracking the rotational speed of the driving wheels of the mowing robot requires both strong robustness and real-time performance within the allowable range of jittering. For this purpose, inspired by the literature [40], this work developed an optimized FPRRL driving motor sliding mode control algorithm, which obtained better control performance. At the same time, a double-closed loop was included to establish a new sliding mode control strategy, which aimed toaccurately track the predetermined trajectory of the mowing robot. This work made the following main contributions:

1) On the basis of the original FPEEL, a new reaching term was added without changing the original parameters, which reduced the arrival time and improved the robustness.

2) Considering the unmodeled disturbance and external disturbance of the system, an extended state observer was designed. An adaptive compensation term for external disturbance was therefore introduced into the control law to improve the robustness of the system.

3) A double closed-loop sliding mode controller was set up to ensure finite-time convergence and realize the tracking of the predetermined trajectory of the lawnmower robot.

The main structure of this paper is as follows: Section 2 describes the system as a whole; Section 3 elaborates the modeling of the lawn mower, the design of the extended state observer, the derivation process of the trajectory tracking controller and the stability proof; Section 4 discusses the simulation results; Section 5 gives the conclusion.

II. SYSTEM OVERVIEW

The mowing robot mobile platform studied in this paper worked with a three-wheel working structure, in which the front wheel was the guide, and the rear two wheels were the driving wheels, with the steering to be realized by differential driving. The driving wheel was driven by two DC motors, and the speed was fed back through the encoder; the position of the body was given by the positioning system.

To realize the tracking of the desired trajectory, the control system was expected to give the output voltage of the driving motor of the mowing robot. To achieve this goal, the desired trajectory was asked to be given in first place. The angular velocity and linear velocity control laws were estimated by the kinematic controller. Subsequently, the voltage output of the driving wheel was estimated by the speed tracking controller in order to form a closed loop. In this way, controllability of the voltage, and thus tracking of the desired trajectory, was fixed. The process is shown in Figure 1. $\boldsymbol{p_d}$ and $\boldsymbol{p}$ are respectively the expected state vector and actual state vector of mowing robot (including position and angle information), U_l, U_r is the output voltage of the left and right wheel drive motors, n_l, n_r is the left and right wheel speeds.

III. DESIGN THE CONTROL ALGORITHM

The algorithm part of this paper includes the kinematic model, the derivation of the motor drive model, the design of the extended state observer, the design of the kinematics controller, the deduction of the speed control algorithm of the driving wheel motor based on the IFPRRL sliding mode control and its stability proof.

A. KINEMATICS MODELING

Kinematics model is the basis for studying the trajectory tracking of sports robots [41]. By establishing a Cartesian coordinate system (as shown in Figure 2), the actual position of the robot may be determined by combining the angular velocity and linear velocity of the motion.

The state of the lawn mower robot is represented by the coordinates of the center M and the heading angle θ. Let the state vector $\boldsymbol{p} = [x\ y\ \theta]$, $\boldsymbol{q} = [v\ \omega]$ be the speed vector of the mowing robot. The relationship between $\boldsymbol{p}$ and $\boldsymbol{q}$ can be expressed as

$$\begin{cases} \dot{x} = v\cos\theta \\ \dot{y} = v\sin\theta \\ \dot{\theta} = \omega \end{cases} \tag{1}$$

Written in matrix form

$$\dot{\boldsymbol{p}} = \begin{bmatrix} \dot{x} \\ \dot{y} \\ \dot{\theta} \end{bmatrix} = \begin{bmatrix} \cos\theta & 0 \\ \sin\theta & 0 \\ 0 & 1 \end{bmatrix} \boldsymbol{q}^T \tag{2}$$

For the kinematics model, the system inputs are linear velocity v and angular velocity ω, while for the mowing robot, there are only two drive motors that can be directly controlled. So, it is necessary to design a kinematics controller to transform the system control v and ω The relationship between the linear velocity v and the angular velocity ω into controlling the rotation speed of the two driving wheels of the robot.

Note: M is the geometric center point of the robot, x, y, θ are the current horizontal and vertical axis positions and angles, v is the robot's forward speed, v_l and v_r are the linear velocities of the left and right wheels, R is the radius of the

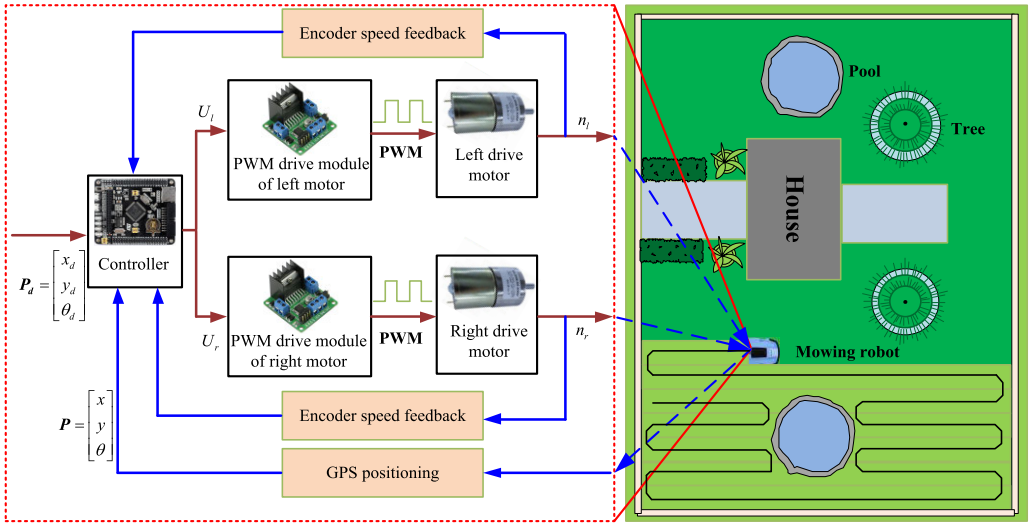

FIGURE 1. Overall block diagram of the control system.

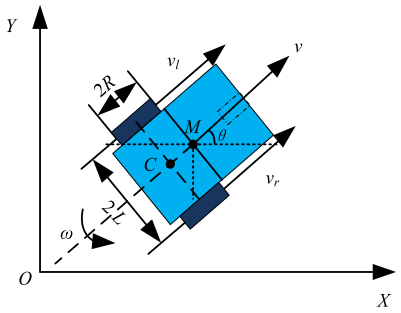

FIGURE 2. Schematic diagram of the Cartesian coordinates of the lawn mower robot.

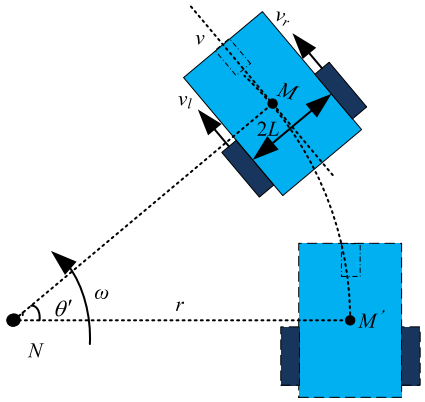

FIGURE 3. Schematic diagram of robot steering.

driving wheels, ω is the angular velocity of rotation, $2L$ is the distance between the driving wheels, C is the middle point of the driving wheel.

In the figure 3, the center of the steering circle of the robot is N, the geometric center is M, the angle of rotation of the robot is θ', and the distance between the two wheel axes is $2L$, OM is the turning radius r. The relationship between the linear velocity v and the linear velocity of the left and right driving wheel v_l, v_r is

$$v = \frac{v_l + v_r}{2} \tag{3}$$

The angular velocity of the left and right wheels are the same, so

$$\dot{\theta}' = \omega = \frac{v}{r} = \frac{v_l}{r - L} = \frac{v_r}{r + L} \tag{4}$$

Thus the relation ship of the angular velocity ω and v, v_r is obtained

$$\omega = \frac{v_r - v_l}{2L} \tag{5}$$

Combining (3) and (5), we can get the relationship between $\boldsymbol{q}$ and v_l, v_r

$$\boldsymbol{q}^T = \frac{1}{2}\begin{bmatrix} 1 & 1 \\ -\frac{1}{L} & \frac{1}{L} \end{bmatrix}\begin{bmatrix} v_l \\ v_r \end{bmatrix} \tag{6}$$

Substitute (3) and (5) into equation (2) to obtain the relationship between the state of the lawn mower robot and the rotation speed of the left and right wheels.

$$\begin{bmatrix} \dot{x} \\ \dot{y} \\ \dot{\theta} \end{bmatrix} = \begin{bmatrix} \frac{R}{2}\cos\theta & \frac{R}{2}\cos\theta \\ \frac{R}{2}\sin\theta & \frac{R}{2}\sin\theta \\ -\frac{R}{2L} & \frac{R}{2L} \end{bmatrix}\begin{bmatrix} n_l \\ n_r \end{bmatrix} \tag{7}$$

B. MODEL OF MOTOR DRIVE

The mowing robot used in this work was equipped with a permanent magnet DC motor as the drive motor, which is a device that converts electrical energy into mechanical energy through magnetic coupling. There were two essential parts:

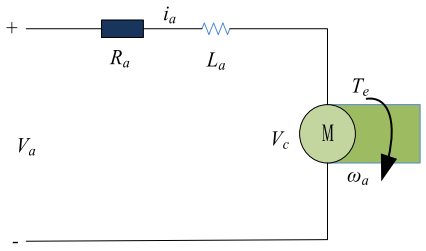

FIGURE 4. Equivalent circuit diagram.

the rotor (or armature) and the stator. The armature rotated in the stator frame of the motor [42]. Its equivalent circuit diagram is shown as in Fig. 4. Where R_a is the total resistance of the armature circuit (including the internal resistance of the power electronic device and the resistance connected in the main circuit), which is a constant, V_c is the back electromotive force generated by the internal coil when the motor is working, V_a is the voltage across the motor, L_a is the total inductance of the main circuit and other inductors connected to it, T_e is the electromagnetic torque, ω_a angular speed of rotor rotation, i_a armature circuit current.

Evidently, when the load is added, the speed of the motor will decrease as the load increases. To make sure that the motor runs stably and safely at the given speed, the motor operation process was analyzed in depth so as to work out the motor modeling and dynamic structure design.

According to the motor model, the voltage balance equation of the main circuit is established as follows

$$V_a = V_{R_a} + V_{L_a} + V_c \tag{8}$$

where V_{R_a} and V_{L_a} are the voltage across R_a, L_a; V_{R_a}, V_{L_a} and V_c are calculated by equation (9).

$$\begin{cases} V_{R_a} = i_a R_a \\ V_{L_a} = L_a \dfrac{d}{dt} i_a \\ V_c = k_v \omega_a \end{cases} \tag{9}$$

where k_v is the speed constant determined by the magnetic flux density of the permanent magnet, the number of rotor windings, and the physical properties of the iron core.

Substituting (9) into (8) to get

$$V_a = i_a R_a + L_a \frac{d}{dt} i_a + k_v \omega_a \tag{10}$$

Then operate the motor torque balance equation, we get

$$T_e = T_{\omega'} + T_\omega + T_L \tag{11}$$

where T_e is the electromagnetic torque of the motor, $T_{\omega'}$ is the torque that drives the acceleration of the rotor, T_ω is the torque generated by the rotor speed, and T_L is the load torque of the motor.

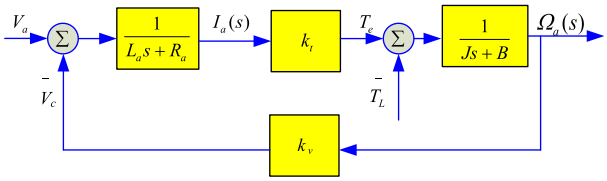

FIGURE 5. Simulation structure diagram of permanent magnet DC motor.

The parts in the equation (11) are

$$\begin{cases} T_e = k_t i_a \\ T_{\omega'} = J \dfrac{d}{dt} \omega_a \\ T_\omega = B \omega_a \end{cases} \tag{12}$$

where k_t is the torque constant determined by the magnetic flux density of the permanent magnet, the number of rotor windings and the physical properties of the iron core, J is the moment of inertia of the rotor and motor load, and B is the damping constant of the entire mechanical rotating system.

Substituting (12) into (11) to get

$$k_t i_a = J \frac{d}{dt} \omega_a + B \omega_a + T_L \tag{13}$$

Combine (11) and (13) to get a complete description of the DC motor:

$$\begin{cases} \dfrac{d}{dt} i_a = -\dfrac{R_a}{L_a} i_a - \dfrac{k_v}{L_a} + \dfrac{V_a}{L_a} \\ \dfrac{d}{dt} \omega_a = \dfrac{k_t}{J} i_a - \dfrac{B}{J} \omega_a - \dfrac{T_L}{J} \end{cases} \tag{14}$$

Laplace transformation is performed on equation (14) to obtain

$$\begin{cases} sI_a(s) - I_a(0) = -\dfrac{R_a}{L_a} I_a(s) - \dfrac{k_v}{L_a} \Omega_a(s) + \dfrac{1}{L_a} V_a(s) \\ s\Omega_a(s) - \Omega_a(0) = \dfrac{k_t}{J} I_a(s) - \dfrac{B}{J} \Omega_a(s) - \dfrac{1}{J} T_L(s) \end{cases} \tag{15}$$

If the disturbance around the steady state is considered, and the initial condition of the motor is assumed to be zero, all variables refer to the offset from the reference state, and the above equation is to become

$$\begin{cases} I_a(s) = \dfrac{-k_v \Omega_a(s) + V_a(s)}{L_a s + R_a} \\ \Omega_a(s) = \dfrac{k_t I_a(s) - T_L(s)}{Js + B} \end{cases} \tag{16}$$

Counting on the above equation, the simulation structure diagram of the permanent magnet DC motor can be drawn, as shown in Figure 5.

From the above, the transfer function of the entire motor is:

$$G(s) = \frac{\Omega_a(s)}{V_a(s)} = \frac{k_t}{L_a J s^2 + (R_a J + L_a B)s + R_a B + k_t k_v} \tag{17}$$

According to formula (17), the state space equation of the DC motor drive model is written as:

$$\begin{cases} \dot{x}_1 = x_2 \\ \dot{x}_2 = a x_2 + b x_1 + c u(t) + d(t) \end{cases} \tag{18}$$

where $a = -(R_aJ + L_aB)/(L_aJ)$, $b = -(r_aB + k_vk_t)/(L_aJ)$, $c = k_t/(L_aJ)$, x_1 and x_2 are the rotational angular velocity and rotational angular acceleration of the motor respectively, $u(t)$ is the control voltage input, and $d(t)$ is the uncertainty disturbance of the system.

C. EXTENDED STATE OBSERVER

Since the total uncertainty disturbance $d(t)$ in the system (18) was unknown, it was necessary to estimate it. ESO was a novel observation algorithm that was responsible for online estimation of internal and external disturbances [43].

Define new state variables $x_1^* = x_1$, $x_2^* = x_2$, $x_3^* = d(t)$, and get a new state space equation (19):

$$\begin{cases} \dot{x}_1^* = x_2^* \\ \dot{x}_2^* = ax_2^* + bx_1^* + cu(t) + x_3^* \\ \dot{x}_3^* = \dot{d}(t) \end{cases} \tag{19}$$

To obtain an estimate of the unknown disturbance d(t), a third-order ESO extended state observer (20) was designed:

$$\begin{cases} \dot{\hat{x}}_1^* = \hat{x}_2^* - \beta_1\left(\hat{x}_1^* - x_1^*\right) \\ \dot{\hat{x}}_2^* = \hat{x}_3^* - \beta_2\left(\hat{x}_1^* - x_1^*\right) + b\hat{x}_1^* + a\hat{x}_2^* + cu(t) \\ \dot{\hat{x}}_3^* = -\beta_3\left(\hat{x}_1^* - x_1^*\right) \end{cases} \tag{20}$$

where $\hat{x}_1^*, \hat{x}_2^*, \hat{x}_3^*$ are the estimated values of state variables x_1^*, x_2^*, x_3^* respectively, β_1, β_2, β_3 is an adjustable state observer parameter.

Define estimation error $\widehat{e}_1 = \hat{x}_1^* - x_1^*$, $\widehat{e}_2 = \hat{x}_2^* - x_2^*$, $\widehat{e}_3 = \hat{x}_3^* - x_3^*$, i.e.

$$\begin{cases} \dot{\widehat{e}}_1 = -\beta_1\widehat{e}_1 + \widehat{e}_2 \\ \dot{\widehat{e}}_2 = (b - \beta_2)\widehat{e}_1 + a\widehat{e}_2 + \widehat{e}_3 \\ \dot{\widehat{e}}_3 = -\beta_3\widehat{e}_1 - \dot{d}(t) \end{cases} \tag{21}$$

Let the matrices $A = \begin{bmatrix} -\beta_1 & 1 & 0 \\ b - \beta_2 & a & 1 \\ -\beta_3 & 0 & 0 \end{bmatrix}$, $B = \begin{bmatrix} 0 & 0 & -1 \end{bmatrix}^T$,

Get

$$\dot{\widehat{e}}_0 = A\hat{e} + B\dot{d}(t) \tag{22}$$

The characteristic polynomial of matrix A is as follows:

$$f(\lambda) = \lambda^3 + a_2\lambda^2 + a_1\lambda + a_0 \tag{23}$$

where $\begin{cases} a_2 = \beta_1 - a \\ a_1 = \beta_2 - b - a\beta_1 \\ a_0 = \beta_3 \end{cases}$.

When using the Routh–Hurwit stability criterion to judge the convergence of $\widehat{e}_o$, it was necessary to ensure that all the eigenvalues of the characteristic polynomial had negative real parts.Introduce ω_0 as the bandwidth of ESO, let

$$\begin{cases} \beta_1 = 3\omega_o + a \\ \beta_2 = 3\omega_o^2 + 3a\omega_o + a^2 + b \\ \beta_3 = \omega_o^3 \end{cases} \tag{24}$$

That is, the characteristic polynomial becomes

$$f(\lambda) = (\lambda + \omega_o)^3 = \lambda^3 + 3\omega_o\lambda^2 + 3\omega_o^2\lambda + \omega_o^3 \tag{25}$$

The three eigenvalues were all $-\omega_o$, so the parameter $\omega_o > 0$ was selected to ensure that the eigenvalues of the characteristic polynomial all had negative real parts, that is, when $t \to \infty$, $\widehat{e} \to 0$. In summary, the estimated value of the disturbance is $\widehat{d}(t)$, $\widehat{d}(t) = \hat{x}_3^*$

D. DOUBLE CLOSED-LOOP SLIDING MODE CONTROLLER

The lawnmower robot is a multi-variable and strongly coupled nonlinear underactuated control system, which has such disadvantages as the changing terrain of the working environment, the intricate obstacles, and the difficulty in establishing the mathematical model accurately. challenge. To deal with the above problems, this work designed a tracking control method in a double closed-loop sliding mode based on ESO. The control block diagram is shown in Figure 6. In the figure, x_d, y_d are the direction expected values of x and y, e_x, e_y is the error between the expected value and the true value of the x-direction and y-direction; θ_d is the expected angle, v_d, w_d are the expected values of velocity and angular velocity, n_{ld}, n_{rd} are the expected rotational speeds of the left and right wheels, respectively; $d(t)$ is system uncertainty disturbance, $\widehat{d}(t)$ is $d(t)$ observed value.

1) KINEMATICS CONTROLLER

According to the kinematic equation of the lawn mower robot, there are 2 degrees of freedom, and the model output is 3 variables. The model is an under-actuated system, which can only make the active tracking of 2 variables, and the remaining variables are in a follow-up or stabilized state. This control is a trajectory tracking problem, that is, by designing a control law $\boldsymbol{q} = [v\ \omega]$ to achieve the tracking of the position of the mobile robot $[x\ y]$, and realize the follow-up of the included angle θ. Therefore, the error model can be decomposed into error of position subsystem and error of angular velocity subsystem [44].

First, by designing the position control law v, the position $[x\ y]$ take the ideal trajectory as $[x_d y_d]$

$$\begin{cases} \dot{x}_\mathrm{e} = v\cos\theta - \dot{x}_\mathrm{d} \\ \dot{y}_\mathrm{e} = v\sin\theta - \dot{y}_\mathrm{d} \end{cases} \tag{26}$$

where $x_\mathrm{e} = x - x_\mathrm{d}$, $y_e = y - y_\mathrm{d}$. Take

$$\begin{cases} v\cos\theta = u_1 \\ v\sin\theta = u_2 \end{cases} \tag{27}$$

For $\dot{x}_\mathrm{e} = v\cos\theta - \dot{x}_\mathrm{d}$, take the sliding mode function $s_1 = x_e$, then $\dot{s}_1 = \dot{x}_\mathrm{c} = u_1 - \dot{x}_\mathrm{d}$, take $\dot{s}_1 = -\alpha\tanh(k\eta)$.

Therefore, the design control law is:

$$u_1 = \dot{x}_\mathrm{d} - a_1\tanh(b_1s_1), \quad (a_1 > 0, b_1 > 0) \tag{28}$$

Stability proof: $\dot{s}_1 = -a_1\tanh(b_1s_1)$, take $V_x = 1/2s_1^2$, then $\dot{V}_x = s_1\dot{s}_1 = -s_1a_1\tanh(b_1s_1)$, $x\tanh(x) = x(\mathrm{e}^x - \mathrm{e}^{-x})/$

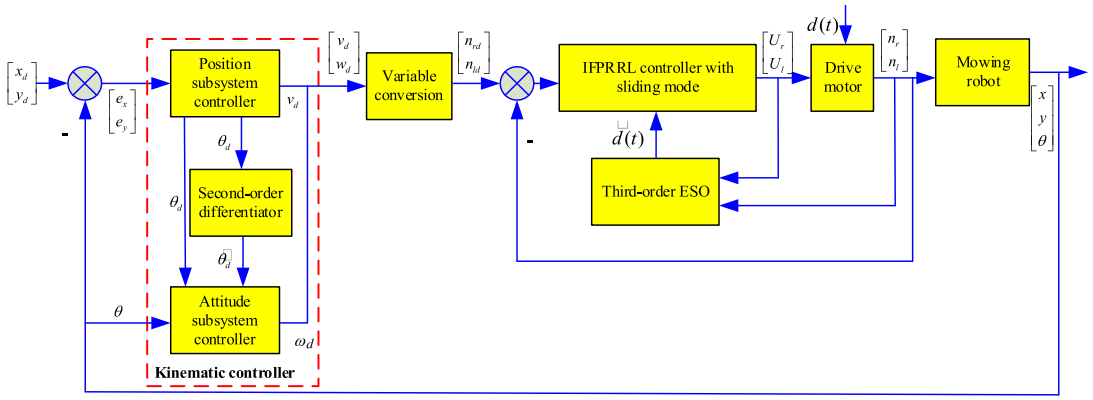

FIGURE 6. Diagram of control block.

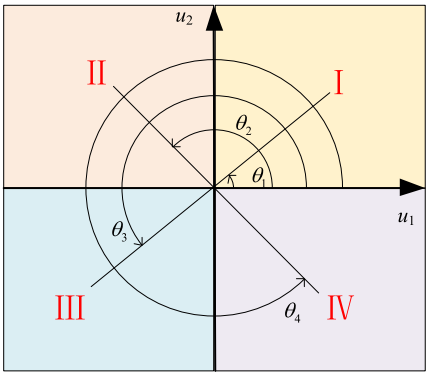

FIGURE 7. Schematic diagram of the quadrant of θ.

$(e^x + e^{-x}) \geqslant 0$, and $a_1 > 0, b_1 > 0$, thus $s_1 a_1 \tanh(b_1 s_1) \geq 0$, so $\dot{V}_x \leq 0$. If and only if $s_1 = 0$, $\dot{V}_x = 0$. Therefore, the system was asymptotically stable.

Similarly, for $\dot{y}_e = v \sin\theta - \dot{y}_d$, take the sliding mode function $s_2 = y_e$, then take $\dot{s}_2 = -\alpha \tanh(k\eta)$ for $\dot{s}_2 = \dot{y}_c = u_2 - \dot{y}_d$, so the design control law is:

$$u_2 = \dot{y}_d - a_2 \tanh(b_2 s_1), \quad (a_2 > 0, b_2 > 0) \tag{29}$$

Stability proof: $\dot{s}_2 = -a_2 \tanh(b_2 s_2)$, take $V_y = 1/2 s_2^2$, then $\dot{V}_y = s_2 \dot{s}_2 = -s_2 a_2 \tanh(b_2 s_2)$, $x \tanh(x) = x(e^x - e^{-x})/(e^x + e^{-x}) \geqslant 0$, and $a_2 > 0, b_2 > 0$, so $s_2 a_2 \tanh(b_2 s_2) \geq 0$, $\dot{V}_y \leq 0$, when And only when $s_1 = 0$, $\dot{V}_y = 0$. Therefore, the system is asymptotically stable.

It can be seen from (27) that the value of θ can be obtained from u_1 and u_2. From Figure 2, θ is a continuously changing value, and the value range should be $(0 + 2n\pi, 2\pi + 2n\pi)$ (n was the period, and $n \in Z$). To obtain the continuously changing value of θ, the value of θ was divided into four quadrants. As shown in Figure 7, the horizontal and vertical coordinates in the figure are u_1 and u_2 *respectively*, θ_1, θ_2, θ_3, and θ_4 are respectively θ schematic angles at I, II, III, IV quadrants.

For this, θ could be obtained as follows

$$\theta = 2n\pi + \begin{cases} \arctan(u_2/u_1), & (u_1 > 0, u_2 > 0) \\ \arctan(u_1/|u_2|) + 0.5\pi, & (u_1 < 0, u_2 > 0) \\ \arctan(|u_2|/|u_1|) + \pi, & (u_1 < 0, u_2 < 0) \\ \arctan(|u_1|/|u_2|) + 1.5\pi, & (u_1 > 0, u_2 < 0) \\ 0, & (u_1 > 0, u_2 = 0) \\ 0.5\pi, & (u_1 = 0, u_2 > 0) \\ \pi, & (u_1 < 0, u_2 = 0) \\ 1.5\pi, & (u_1 = 0, u_2 < 0) \end{cases} \tag{30}$$

In the equation, the first four cases correspond to the calculation formulas of θ when the four quadrants θ_1, θ_2, θ_3 and θ_4 respectively from top to bottom, and the last four cases are respectively the θ calculation formula corresponding to the four-part coordinate axis. It is worth noting here that the initial value of n is 0. When θ changed from the quadrant I to quadrant IV, the value of n was incremented by 1. Conversely, when θ changed from the quadrant IV to quadrant I, the value of n was decremented by 1.

θ obtained by formula (30) is the angle required by the position control law formulas (28) and (29). If θ was equal to θ_d, then the ideal trajectory tracking control law could be realized. In reality, θ and θ_d cannot be exactly the same, especially the initial stage of control being very different. This may cause the entire closed-loop control system to fall in an unstable state.

For this reason, the angle θ obtained by formula (29) may be regarded as an ideal value, that is, take

$$\theta_d = 2n\pi + \begin{cases} \arctan(u_2/u_1), & (u_1 > 0, u_2 > 0) \\ \arctan(u_1/|u_2|) + 0.5\pi, & (u_1 < 0, u_2 > 0) \\ \arctan(|u_2|/|u_1|) + \pi, & (u_1 < 0, u_2 < 0) \\ \arctan(|u_1|/|u_2|) + 1.5\pi, & (u_1 > 0, u_2 < 0) \\ 0, & (u_1 > 0, u_2 = 0) \\ 0.5\pi, & (u_1 = 0, u_2 > 0) \\ \pi, & (u_1 < 0, u_2 = 0) \\ 1.5\pi, & (u_1 = 0, u_2 < 0) \end{cases} \tag{31}$$

Thus, according to formula (27), the actual position control law can be obtained as

$$v = \begin{cases} \dfrac{u_1}{\cos\theta_{\mathrm{d}}}, & \theta_{\mathrm{d}} \neq K\pi + \dfrac{\pi}{2} \\ \dfrac{u_2}{\sin\theta_{\mathrm{d}}}, & \theta_{\mathrm{d}} = K\pi + \dfrac{\pi}{2}, \end{cases} \quad K \in Z \tag{32}$$

In reality, the difference between θ and θ_d may lead to an inaccurate position control law, resulting in the instability of the entire closed-loop system. Therefore, it is necessary to design a faster algorithm in attitude control law than the position control law to make θ track θ_d in a quicker way.

The previous task guarantees (x, y) tracking. Secondly, the accurate tracking of θ makes it necessary to create the attitude control law w, so as to see the angular velocity tracking.

Take $\theta_e = \theta - \theta_{\mathrm{d}}$, sliding mode function $s_3 = \theta_e$. Then:

$$\dot{s}_3 = \dot{\theta}_{\mathrm{e}} = \omega - \dot{\theta}_{\mathrm{d}} \tag{33}$$

Create the attitude control law as:

$$\omega = \dot{\theta}_{\mathrm{d}} - k_3 s_3 - \eta_3 \ \mathrm{sgn}\ s_3 \tag{34}$$

where k_3 and η_3 are constants, and $k_3 > 0$, $\eta_3 > 0$.

Then $\dot{s}_3 = -k_3 s_3 - \eta_3 \ \mathrm{sgn}\ s_3$, take $V_\theta = 1/2 s_3^2$, then $\dot{V}_\theta = s_3\dot{s}_3 = -k_3 s_3^2 - \eta_3|s_3| \leqslant -k_3 s_3^2$, that is, $\dot{V}_\theta \leqslant -2k_3 V_\theta$, so, the system was asymptotically stable.

The designed closed-loop system is composed of inner and outer loops. The inner loop is the attitude subsystem, including an attitude subsystem sliding mode controller; the outer loop is the position subsystem to generate the intermediate command signal θ_d, which is passed to the inner loop system. The inner loop system follows the sliding mode control law to track this intermediate command signal. The closed loop system is structured as shown in the red box in Figure 6.

Since $\dot{\theta}_d$ needs to be implemented when designing the inner loop controller, a continuous value is required for v_d, so that the control law u_1 and u_2 are continuous values. Therefore, u_1 and u_2 are not allowed to include switching functions.

In the attitude control law equation (34), the derivation of $\dot{\theta}_d$ is needed. This is a complicated process. In this work, a linear second-order differentiator was merited to implement $\dot{\theta}_d$.

$$\begin{cases} \dot{\xi}_1 = \xi_2 \\ \dot{\xi}_2 = -2A^2\left(\xi_1 - n(t)\right) - A\xi_2 \\ \psi = \xi_2 \end{cases} \tag{35}$$

In the equation, the input signal to be differentiated is $n(t)$, ξ_1 is to track the signal, and ξ_2 is the estimation of the first derivative of the signal, A is the differentiator parameter, the initial value of the differentiator is $\xi_1(0) = 0$, $\xi_2(0) = 0$.

To achieve stable inner-loop control with sliding mode, this work was performed by way of making the inner-loop convergence speed greater than the outer-loop convergence speed to achieve θ fast tracking θ_d, thus ensuring the stability of the closed-loop system. In this system, the control gain coefficients of the inner and outer loops were by adjusted. This is a guarantee that the convergence speed of the inner loop is greater than that of the outer loop.

2) SLIDING MODE CONTROLLER BASED ON IFPRRL

As aforementioned, we have got the control laws v and ω, and the left and right wheel speeds could be obtained by formula (7) n_l, n_r. The issue on how to make the left and right wheel drive motors of the lawn mower robot track n_l, n_r stood up to be discussed below. The driving motors were the same to the left wheel and the right wheel, and won't be described separately in this paper.

According to the state space equation (18), select the error $n_e = x_{1d} - x_1$, where x_{1d} is the set value of the rotational angular velocity. The first step is to determine the sliding mode surface function s_4, as shown in formula (36)

$$s_4 = c_1 n_e + \dot{n}_e \tag{36}$$

To ensure the existence of the designed sliding surface, c_1 needs to satisfy the Hurwitz condition, that is, $c_1 > 0$. Taking the derivative of s_4, we get

$$\dot{s}_4 = c_1\dot{n}_e + \ddot{x}_{1d} + ax_2 + bx_1 - cu - \widehat{d}(t) \tag{37}$$

The FPRRL proposed by [40] is as follows:

$$\dot{s}_4 = -\frac{k}{\varrho + \sigma^{|s_4|}}\,|s_4|^{\varpi}\ sign\,(s_4) \tag{38}$$

where $0 < \varrho < 1, 0 < \sigma < 0.1, 0 < \varpi < 1, k > 0$, and the reaching law is, by designing a scaling function, integrated into the control structure so that the controller gain varies with the magnitude of the switching function. Thus good robustness and arrival time were obtained.

Although this reaching law suppressed jittering well, it had a better arrival time for systems with small step changes. Nonetheless, when applied to a system with large step changes, a larger k value had to be selected to ensure the arrival time, except for an excessively large k that may lead to increased jittering. Therefore, it is crucial to reduce the arrival time within a reasonable range. In this regard, this work managed to get an improved FPRRL, which is shown in formula (39) after the improvement

$$\dot{s}_4 = -\frac{k}{\varrho + \sigma^{|s_4|}}\,|s_4|^{\varpi}\ sign\,(s_4) - \frac{\varepsilon}{\varrho + \sigma^{|s_4|}}s_4 \tag{39}$$

where $\varepsilon > 0$ and $\varepsilon/(\varrho+\sigma^{|s_4|})$ are strictly positive, so it has no effect on the stability of the system. In the improved reaching law, a new exponential approach term $-(\varepsilon/(\varrho + \sigma^{|s_4|}))s_4$ is added, which is different from the conventional exponential term $-\varepsilon s_4$ [38], compared to $0 < \varrho < 1, 0 < \sigma < 0.1$, in the new exponential approach term. Therefore $0 < \sigma^{|s_4|} \leq 1$, the larger the $|s_4|$, the smaller the value of $\sigma^{|s_4|}$, and the larger the $\varepsilon/(\varrho + \sigma^{|s_4|})$. Conversely, the smaller the $|s_4|$, the smaller the value of $\varepsilon/(\varrho + \sigma^{|s_4|})$. With the help of the proposed methodology, Figure (8) depicts the comparison of coefficients for exponential approach term and conventional exponential term.

From the figure, the approach process is described as follows:

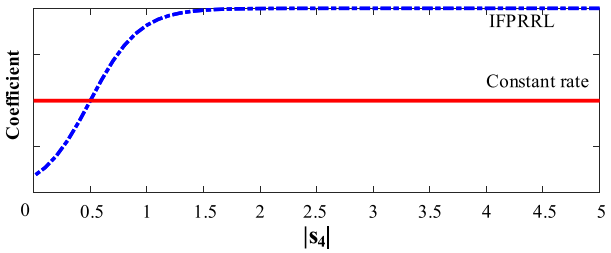

FIGURE 8. Comparison of the exponential approach term in this paper and the conventional exponential term.

1) In the initial stage of control, $|s_4|$ was the largest, $\varepsilon/(\varrho+\sigma^{|s_4|})$ was the largest, and s_4 could move to the sliding surface at the maximum rate.

2) In the middle stage of control, when $\varepsilon/(\varrho+\sigma^{|s_4|})=\varepsilon$ was equal to εs.

3) $|s_4|$ gradually decreased, $\sigma^{|s_4|}$ approached 1, and $\varepsilon/(\varrho+\sigma^{|s_4|})$ became smaller, so as to delay the approach speed and ensure a smoother approach to the sliding surface.

Putting the reaching law (39) into formula (37), we get (40):

$$c_1\dot{n}_e+\ddot{x}_{1d}+ax_2+bx_1-cu(t)-\widehat{d}(t) =-\frac{k}{\varrho+\sigma^{|s_4|}}|s_4|^{\varpi}\,sign\,(s_4)-\frac{\varepsilon}{\varrho+\sigma^{|s_4|}}s_4 \quad (40)$$

Find the control amount $u(t)$ (41)

$$u(t)=\frac{1}{c}(c_1n_e+\ddot{x}_{1d}-ax_2-bx_1-\widehat{d}(t) +\frac{k}{\varrho+\sigma^{|s_4|}}|s_4|^{\varpi}\,sign\,(s_4)+\frac{\varepsilon}{\varrho+\sigma^{|s_4|}}s_4) \quad (41)$$

Proof of Stability: $s_4=c_1n_e+\dot{n}_e$, take $V_{s4}=1/2s_4^2$, then

$$\begin{aligned}\dot{V}_{s4}&=s_4\dot{s}_4\\&=s_4[c_1\dot{n}_e+\ddot{x}_{1d}-ax_2-bx_1-cu(t)-\widehat{d}(t)]\\&=s_4[c_1\dot{n}_e+\ddot{x}_{1d}-ax_2-bx_1-(c_1\dot{n}_e+\ddot{x}_{1d}-ax_2-bx_1-\widehat{d}(t)\\&\quad+\frac{k}{\varrho+\sigma^{|s_4|}}|s_4|^{\varpi}\,sign\,(s_4)+\frac{\varepsilon}{\varrho+\sigma^{|s_4|}}s_4-\widehat{d}(t)]\\&=-s_4\frac{k}{\varrho+\sigma^{|s_4|}}|s_4|^{\varpi}\,sign\,(s_4)-\frac{\varepsilon}{\varrho+\sigma^{|s_4|}}{s_4}^2\end{aligned}$$

Apparently $k/(\varrho+\sigma^{|s_4|})|s_4|^{\varpi}>0$, $-s_4 sign\,(s_4)\le 0$, $\varepsilon/(\varrho+\sigma^{|s_4|})s_4^2\ge 0$, and therefore $\dot{V}_{s4}\le 0$, which indicated that this control law was there as a guarantee to the asymptotic stability of the system.

IV. SIMULATION RESULTS AND ANALYSIS

A. SIMULATION AND ANALYSIS OF DRIVE MOTOR SPEED CONTROL

Firstly, taking the robot-driven DC motor as the controlled object, the correctness and effectiveness of the improved FPRRL sliding mode control algorithm in this paper were verified. The simulation environment was MATLAB2018b,

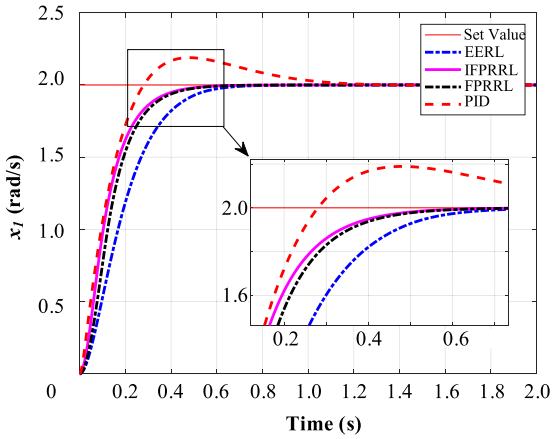

FIGURE 9. Step response curves for different controllers.

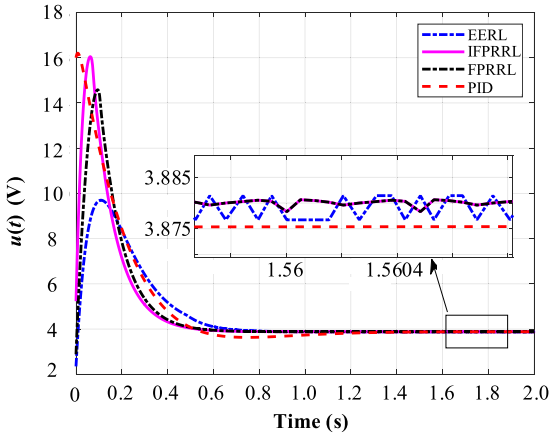

FIGURE 10. Control output for different controllers.

the drive motor parameters were $R_a=2$, $L_a=0.02$H, $J=10.1$ kg.m^2, $k_v=1.8$V/(rad/s), $k_t=17.2$Nm/A, ESO bandwidth $\omega_o=60$. Set the initial speed to 0rad/s and the target speed to 2rad/s. Its speed was regulated, respectively, by means of PID controller, two mature reaching law control methods EERL [38], FPRRL [40] and improved FPRRL. The key formulas and parameter settings used in simulation are shown in Table 1.

Figure9 shows the tracking effect. As evidenced in the figure, the PID control shows a faster rising speed, but the overshoot of 9.45% and the adjustment time of 1.3s produced an unsatisfactory control effect. Except for the PI controller, all three reaching law sliding mode control methods presented similar arrival times, where FPRRL was slightly better than EERL, and the improved FPRRL was slightly better than FPRRL. Note that the improvement here is not an improvement by adjusting the size of the parameters. Rather, a new structure did the job to improve the control performance under similar parameters.

Figure10 shows the output of the controller. The improved FPRRL was compared with the control outputs of the PI,

TABLE 1. Parameter settings.

Control plan	Formula	Parameter
PID	$u(t)=K_p n_e+T_I\int_0^t n_e dt+T_D\frac{dn_e}{dt}$	K_p=8, T_I=30, $T_D=0$
EERL	$\dot{s}_4=-\frac{k}{\delta+(1-\delta)e^{-\alpha\lvert s_4\rvert^p}}\lvert s_4\rvert^{\varpi}sign(s_4)-\varepsilon s_4$	p=10, α = 20, δ =0.1, ϖ =0.3 ε =10, k=0.2
FPRRL	$\dot{s}_4==-\frac{k}{\varrho+\sigma\lvert s_4\rvert}\lvert s_4\rvert^{\varpi}sign(s_4)$	$\varrho=0.1$, $\sigma=0.01$, ϖ =0.3, k=10
Improved FPRRL	$\dot{s}_4=-\frac{k}{\varrho+\sigma\lvert s_4\rvert}\lvert s_4\rvert^{\varpi}sign(s_4)-\frac{\varepsilon}{\varrho+\sigma\lvert s_4\rvert}s_4$	$\varrho=0.1$, $\sigma=0.01$, ε =1, ϖ =0.3, k=10

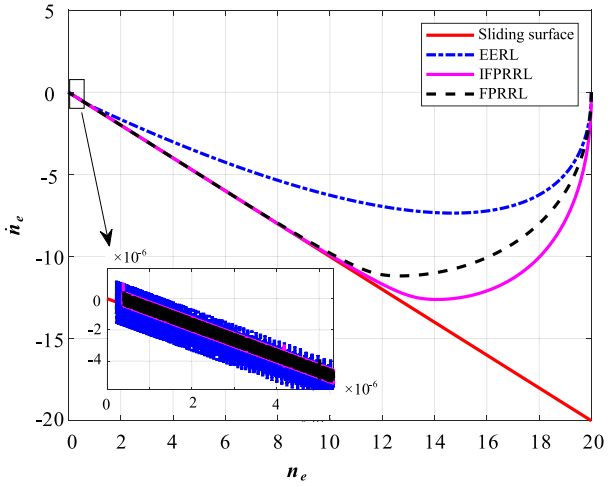

FIGURE 11. Sliding mode motion under different reaching laws.

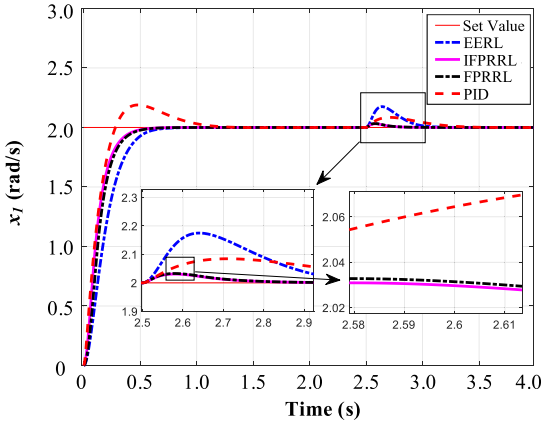

FIGURE 12. Response curves of different controllers under external disturbances.

EERL, FPRRL algorithms. It is plain to see that, except for PI control, jittering exists in all three sliding mode control methods. Among them, the jittering of EERL is the largest, and the amplitude is within ±0.005V. The FPRRL and the improved FPRRL have almost the same jitter amplitude, within ±0.003V. The improved FPRRL reaching law

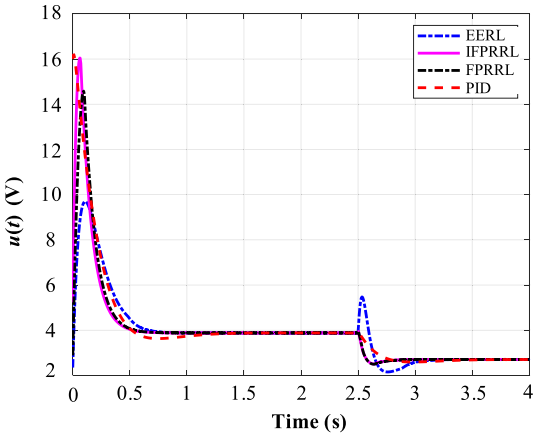

FIGURE 13. Outputs of different controllers under external disturbances.

proposed in this paper made good performance in jittering control. That is, the advantage of low jittering of FPRRL may be maintained on the premise of an optimized arrival time.

Figure11 shows the achievement of three sliding mode surfaces of EERL, FPRRL and improved FPRRL. It can be seen that the improved FPRRL gave the shortest arrival time, followed by FPRRL and finally EERL. As expected, there were sliding modes in all three sliding modes, but the buffeting of FPRRL and improved FPRRL was significantly smaller than that of EERL. The results showed that the improved FPRRL expressed a faster arrival time than the previous one under the premise of similar system robustness and jittering.

B. ROBUSTNESS ANALYSIS OF CONTROLLER UNDER STEP DISTURBANCE

To verify the robustness of the improved FPRRL algorithm, this work made a suddenly increase in the interference at t = 2.5s (formula 42). If the controller was robust enough, it must be able to overcome the disturbance and maintain a good tracking effect.

$$d(t)=\begin{cases}0 & 0\le t<2.5\\ 100 & t\ge 2.5\end{cases} \tag{42}$$

Figure12 is the response curve after applying disturbance, and Figure 13 is the controller output. Obviously, both EERL

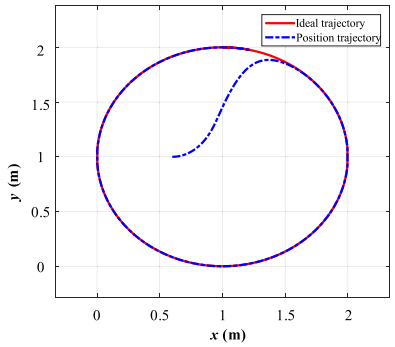

(a) Trajectory tracking

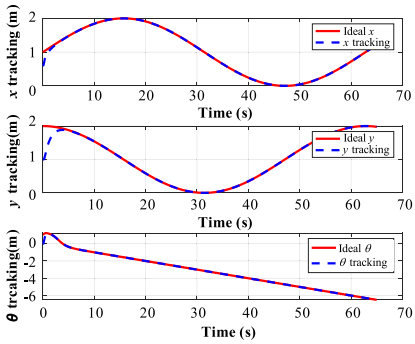

(b) Three-component tracking of x, y, θ

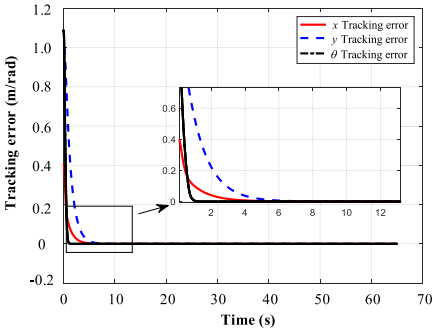

(c) Tracking error of three components of x, y, θ

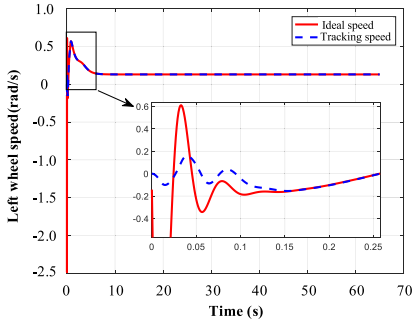

(d) Tracking of left wheel speed

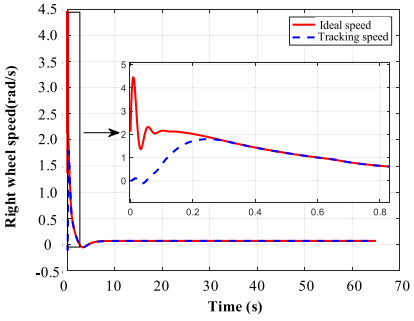

(e) Tracking of right wheel speed

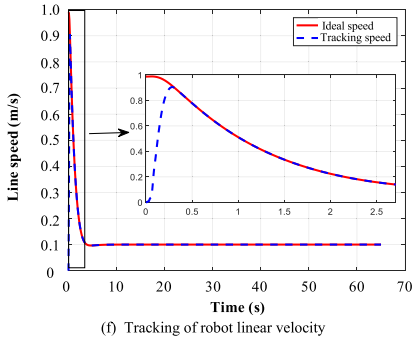

(f) Tracking of robot linear velocity

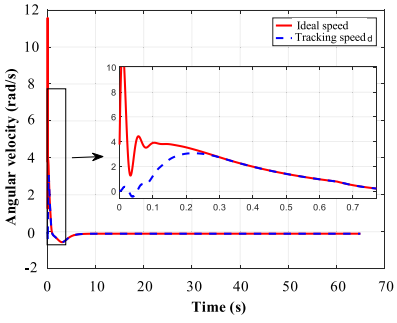

(g) Tracking of robot angular velocity

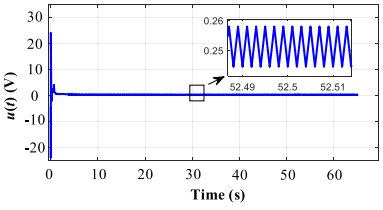

(h) Output of left wheel drive motor

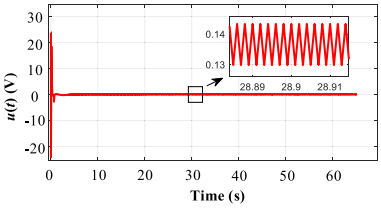

(i) Output of right wheel drive motor

FIGURE 14. **Circular trajectory tracking simulation.**

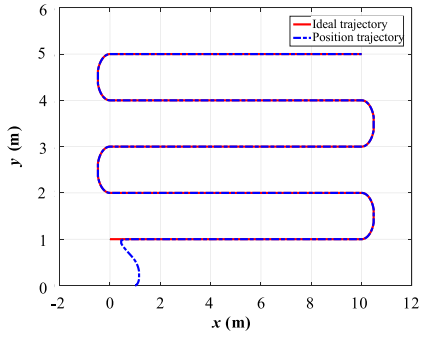

(a) Trajectory tracking

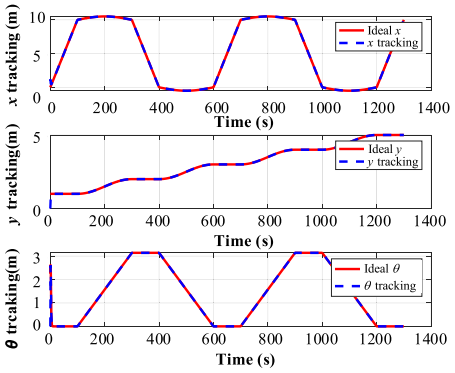

(b) Three-component tracking of x, y, θ

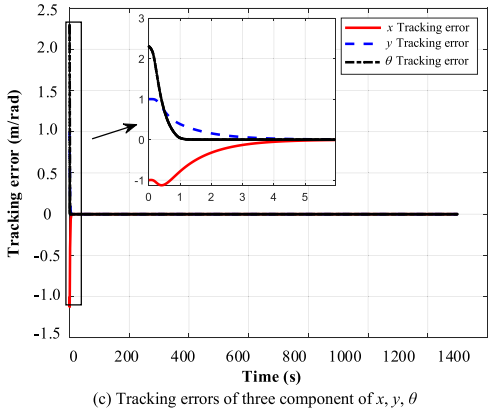

(c) Tracking errors of three component of x, y, θ

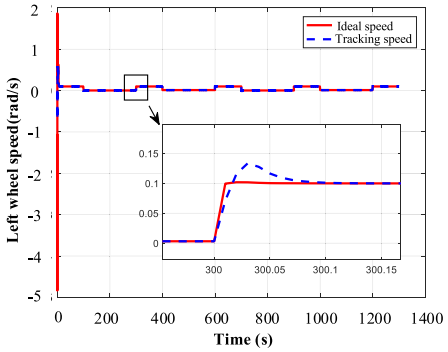

(d) Tracking of left wheel speed

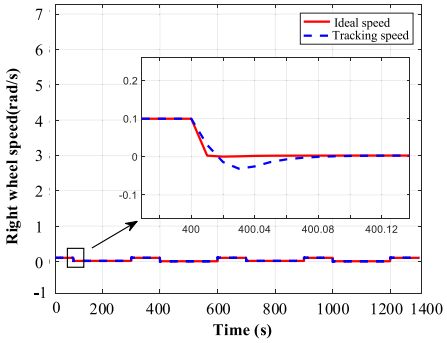

(e) Tracking of right wheel speed

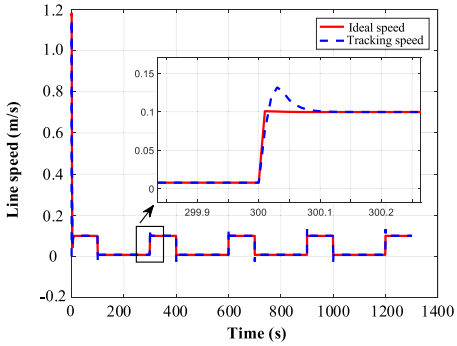

(f) Tracking of robot linear velocity

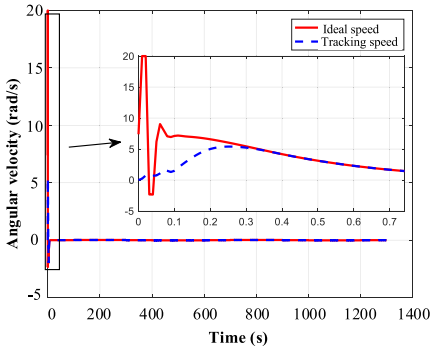

(g) Tracking of robot angular velocity

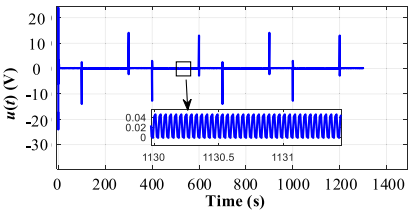

(h) Output of left wheel drive motor

FIGURE 15. Detoured tracking of mowing robot.

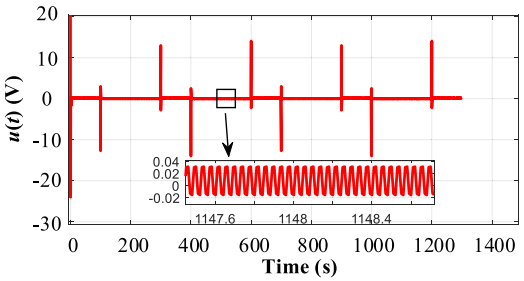

(i) Output of right wheel drive motor

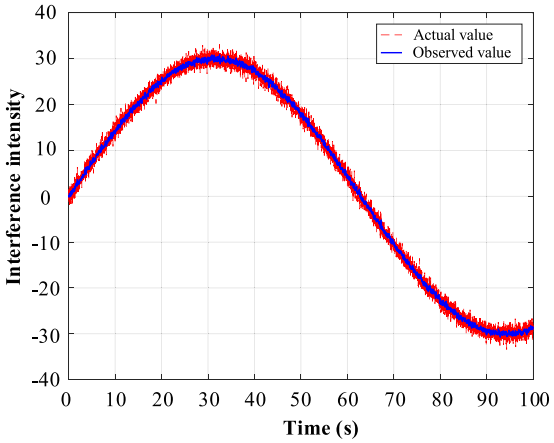

(j) Disturbance of the left wheel

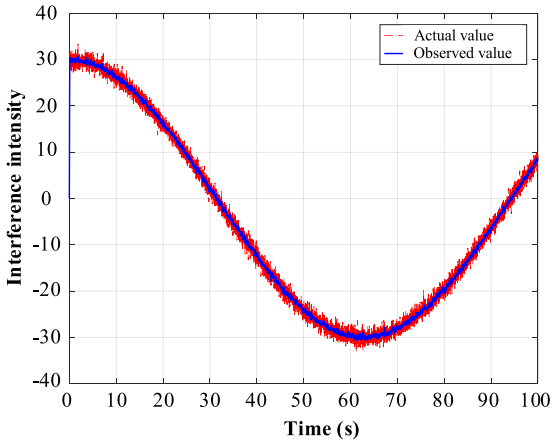

(k) Disturbance of the right wheel

FIGURE 15. ***(Continued.)*** **Detoured tracking of mowing robot.**

and PI controller performance were greatly affected. Among them, the EERL error was the largest, up to 0.17rad, followed by PI control, which also hit 0.085rad. The maximum error between FPRRL and the improved FPRRL was not more than 0.033rad, and the maximum error of the improved FPRRL was slightly lower than that of the FPRRL, and the maximum error was 0.03rad. Additionally, the recovery time from disturbance also varied. The PI controller had the longest adjustment time of 0.826s, followed by EERL with 0.564s, FPRRL with 0.241s, and the improved FPRRL with the shortest adjustment time of 0.235s. The results showed that the algorithm proposed in this paper had improved robustness.

C. SIMULATION AND ANALYSIS

Taking the lawn mower robot as the controlled object, the path tracking simulation experiment was then carried out. Improved FPRRL sliding mode controller used parameter selection as the same as above. The parameters in the motion controller were $a_1 = a_2 = 3$, $b_1 = b_2 = 10$, $a_3 = 3.0$, $b_3 = 0.5$. In the attitude control law, the differentiator parameter was selected as 100. The actual parameters of the robot are as follows: the radius of the driving wheel is 0.1m, the distance between the two wheels is 0.3m, and the distance between the center line of the wheel and the front end is 0.12m.

First select a circular trajectory for tracking. The center of the reference trajectory (desired trajectory) was (0m, 0m), with the radius of 1 m. As shown in formula (43):

$$\begin{cases} x_d = \sin(0.1t) + 1 \\ y_d = \cos(0.1t) + 1 \end{cases} \tag{43}$$

Robot The initial pose of the global coordinate is (x_0, y_0, θ_0) = (0.6m, 1 m, 0rad), the initial linear velocity and steering angle are (v_0, w_0) = (0 m/s, 0 rad/s). The simulation result of circular trajectory tracking is shown in the figure 14 shown.

As indicated in Figure 14, θ_e is stable within 0.01rad after 0.94s, and x_e is within 3.5s After stabilizing within 0.01m, y_e stabilized within 0.01m after 5.34s. The simulation error of the circular arc trajectory of the platform continued to converge with the increase of time, and finally tends to 0. And Fig. 14(h)(i) shows the output jittering of the controller

of the left wheel and the right wheel are both kept within the range of ±0.02V. Under the condition that the initial errors are $x_e = 0.4$m and $y_e = 1$m respectively, the proposed controller, as expected, made the lawnmower robot converge to the desired trajectory smoothly and achieved satisfactory tracking effect. Judging from the tracking situation of θ in Fig. 12(b), θ was continuous during the movement of the robot, which successfully solved the problem of control system jitter caused by the angle flip during the control process.

To simulate the real mowing path, this work picked a 6m × 10m rectangular lawn as the lawn mowing robot's work site, in which the path planning was detoured. The simulation environment and controller parameters were the same as above, and the robot's initial pose $(x_0, y_0, \theta_0) = (1\text{m}, 0\text{ m}, 0\text{rad})$, the initial linear velocity and steering angle were $(v_0, w_0) = (0\text{ m/s}, 0\text{ rad/s})$. Set the starting position of the path as (0m, 1m), the straight line length of the path as 10m, the set speed of the straight line as 0.1m/s, the arc radius as 0.5m, and the turning velocity as app. 0.01m/s, and the whole tracking process was introduced with disturbance (44).

$$\begin{cases} d_l(t) = 30\sin(0.05t) + n(t) \\ d_r(t) = 30\cos(0.05t) + n(t) \end{cases} \tag{44}$$

where $d_l(t)$ is the left wheel interference, $d_r(t)$ is the right wheel interference, $n(t)$ is Gaussian white noise, its amplitude is $[-1,1]$, and the signal-to-noise ratio is 3dB. The tracking effect is shown in Figure 15.

Figure 15 displays that the simulation error of the tracking trajectory continues to converge with time, x_e, y_e, θ_e are kept within the range of 0.01m, 0.01m, 0.01rad, and the time is 3.55s, 5.36s, 0.99s respectively. And look in Figures (h) and (i), the control voltage of the left and right wheels varies little, and the jittering is not greater than ±0.05V. Furthermore, the designed ESO did a good job on observing the interference of the superposition of sinusoidal and Gaussian white noise, and then compensated the controller to ensure the robustness of the system.

The simulation results showed that the sliding mode control with double closed-loop designed in this work came along with several typical advantages, such as real-time performance, robustness and tracking accuracy. When used to track the trajectory of the lawn mowing robot, this proposed methodology was able to satisfy the tracking requirements of the predetermined trajectory, and served as valuable reference for achieving full coverage of the mowing area and reducing missed cuts and re-cuts.

V. CONCLUSION

In this work, the lawnmower robot was regarded as a cascaded system composed of motor drive equations and vehicle body kinematics equations. The whole design was aimed at a sliding mode controller for driving motor and a sliding mode trajectory tracking controller with dual closed-loop for lawn mowing robot. The following conclusions are drawn:

1) In this paper, a new reaching law sliding mode controller is introduced to control the speed of the drive motor through simulation experiments. The results showed that under similar buffeting, the new reaching law got faster arrival time and better robustness than the traditional sliding mode algorithm.

2) For unmodeled disturbances and external disturbances, an extended state observer was developed to achieve effective observation of external disturbances and compensate them in control, further improving the robustness of the system.

3) The sliding mode controller with double closed-loop designed was proven to control the lawn mowing robot to effectively track the circular trajectory. It guaranteed that the error vectors $P_e = (x_e, y_e, \theta_e)$ remaining in the range of (0.01m, 0.01m, 0.01rad) are 3.5s, 5.34s and 0.94s at the time frame, respectively, and finally converged to 0. Accordingly, the control voltage jittering was controlled within ±0.02V.

4) In the scenario where both the left and right wheels were accompanied by the superimposed interference of sine and white noise, the circuitous mowing trajectory was effectively tracked while the tracking error continued to converge with the increase of time. Specifically, x_e, y_e, θ_e kept in the range of 0.01m, 0.01m, 0.01rad at the time frame of 3.55s, 5.36s, 0.99s respectively. The voltage jittering was controlled within ±0.05V, prevailing at anti-interference ability.

REFERENCES

[1] M. Cong, L. G. Jin, and B. Fang, "Intelligent robot mowers: A review," *Robot*, vol. 29, no. 4, pp. 407–416, Apr. 2007.
[2] J. E. Normey-Rico, I. Alcalá, J. Gómez-Ortega, and E. F. Camacho, "Mobile robot path tracking using a robust PID controller," *Control Eng. Pract.*, vol. 9, no. 11, pp. 1209–1214, 2001.
[3] R.-E. Precup and S. Preitl, "Sensitivity analysis of a class of fuzzy controlled mobile robots," *IFAC Proc. Volumes*, vol. 37, no. 16, pp. 115–120, Sep. 2004.
[4] T. Zahid, Z. Kausar, M. F. Shah, M. T. Saeed, and J. Pan, "An intelligent hybrid control to enhance applicability of mobile robots in cluttered environments," *IEEE Access*, vol. 9, pp. 50151–50162, 2021.
[5] Z. P. Jiang and H. Nijmeijer, "Tracking control of mobile robots: A case study in backstepping," *Automatica*, vol. 33, no. 7, pp. 1393–1399, Jul. 1997.
[6] I. Zohar, A. Ailon, and R. Rabinovici, "Mobile robot characterized by dynamic and kinematic equations and actuator dynamics: Trajectory tracking and related application," *Robot. Auton. Syst.*, vol. 59, no. 6, pp. 343–353, Jun. 2011.
[7] L. Enli, J. Wei, W. Yu, J. Zhao, F. Wang, and Y. Liu, "Trajectory tracking algorithm of autonomous mobile platform for animal husbandry environment information monitoring," *Trans. Chin. Soc. Agricult. Eng.*, vol. 34, no. 13, pp. 86–94, Jul. 2018.
[8] K. G. Jolly, R. S. Kumar, and R. Vijayakumar, "An artificial neural network based dynamic controller for a robot in a multi-agent system," *Neurocomputing*, vol. 73, nos. 1–3, pp. 283–294, Dec. 2009.
[9] S. Xu, Y. Ou, J. Duan, X. Wu, W. Feng, and M. Liu, "Robot trajectory tracking control using learning from demonstration method," *Neurocomputing*, vol. 338, pp. 249–261, Apr. 2019.
[10] S. Soyguder, "Intelligent control based on wavelet decomposition and neural network for predicting of human trajectories with a novel vision-based robotic," *Expert Syst. Appl.*, vol. 38, no. 11, pp. 13994–14000, May 2011.
[11] G. P. Moustris and S. G. Tzafestas, "Switching fuzzy tracking control for mobile robots under curvature constraints," *Control Eng. Pract.*, vol. 19, no. 1, pp. 45–53, Jan. 2011.
[12] N. F. Martins, W. C. Celeste, R. Carelli, S. F. Mário, and B. F. Teodiano, "An adaptive dynamic controller for autonomous mobile robot trajectory tracking," *Control Eng. Pract.*, vol. 16, no. 11, pp. 1354–1363, Nov. 2008.
[13] B. S. Park, S. J. Yoo, J. B. Park, and Y. H. Choi, "A simple adaptive control approach for trajectory tracking of electrically driven nonholonomic mobile robots," *IEEE Trans. Control Syst. Technol.*, vol. 18, no. 5, pp. 1199–1206, Sep. 2010.

[14] K. Shojaei, A. M. Shahri, and A. Tarakameh, "Adaptive feedback linearizing control of nonholonomic wheeled mobile robots in presence of parametric and nonparametric uncertainties," *Robot. Comput.-Integr. Manuf.*, vol. 27, no. 1, pp. 194–204, Feb. 2011.
[15] D. Huang, J. Zhai, W. Ai, and S. Fei, "Disturbance observer-based robust control for trajectory tracking of wheeled mobile robots," *Neurocomputing*, vol. 198, no. 19, pp. 74–79, Jul. 2016.
[16] F. Yan, B. Li, W. Shi, and D. Wang, "Hybrid visual servo trajectory tracking of wheeled mobile robots," *IEEE Access*, vol. 6, pp. 24291–24298, 2018.
[17] J.-M. Yang and J.-H. Kim, "Sliding mode control for trajectory tracking of nonholonomic wheeled mobile robots," *IEEE Trans. Robot. Autom.*, vol. 15, no. 3, pp. 578–587, Jun. 1999.
[18] M. Mauder, "Robust tracking control of nonholonomic dynamic systems with application to the bi-steerable mobile robot," *Automatica*, vol. 44, no. 10, pp. 2588–2592, Oct. 2008.
[19] Y. Zhang, G. Liu, and B. Luo, "Finite-time cascaded tracking control approach for mobile robots," *Inf. Sci.*, vol. 284, pp. 31–43, Nov. 2014.
[20] K. Alipour, A. B. Robat, and T. Bahram, "Dynamics modeling and sliding mode control of tractor-trailer wheeled mobile robots subject to wheels slip," *Mechanism Mach. Theory*, vol. 138, pp. 16–37, Aug. 2019.
[21] X. Yang, P. Wei, Y. Zhang, X. Liu, and L. Yang, "Disturbance observer based on biologically inspired integral sliding mode control for trajectory tracking of mobile robots," *IEEE Access*, vol. 7, pp. 48382–48391, 2019.
[22] R. Vilanova and V. M. Alfaro, "Control PID robusto: Una visión panorámica," *Revista Iberoamericana de Automática e Informática Industrial RIAI*, vol. 8, no. 3, pp. 407–416, Sep. 2011.
[23] V. Utkin, "Variable structure systems with sliding modes," *IEEE Trans. Autom. Control*, vol. AC-22, no. 2, pp. 212–222, Apr. 1977.
[24] J. J. Slotine and S. Sastry, "Tracking control of nonlinear systems using sliding surfaces with application to robot manipulator," *Int. J. Control*, vol. 38, no. 2, pp. 465–492, Apr. 1983.
[25] M.-S. Chen, Y.-R. Hwang, and M. Tomizuka, "A state-dependent boundary layer design for sliding mode control," *IEEE Trans. Autom. Control*, vol. 47, no. 10, pp. 1677–1681, Oct. 2002.
[26] S. Seshagiri and H. K. Khalil, "On introducing integral action in sliding mode control," in *Proc. 41st IEEE Conf. Decis. Control*, Jan. 2003, pp. 1473–1478.
[27] P. Kachroo and M. Tomizuka, "Chattering reduction and error convergence in the sliding-mode control of a class of nonlinear systems," *IEEE Trans. Autom. Control*, vol. 41, no. 7, pp. 1063–1068, Jul. 1996.
[28] B. P. Kang and J. L. Ju, "Sliding mode controller with filtered signal for robot manipulators using virtual plant/controller," *Mechatronics*, vol. 7, no. 3, pp. 277–286, Apr. 1997.
[29] G. Bartolini, A. Ferrara, and E. Usai, "Chattering avoidance by second-order sliding mode control," *IEEE Trans. Autom. Control*, vol. 43, no. 2, pp. 241–246, Feb. 1998.
[30] A. Polyakov and A. Poznyak, "Reaching time estimation for 'super-twisting' second order sliding mode controller via Lyapunov function designing," *IEEE Trans. Autom. Control*, vol. 54, no. 8, pp. 1951–1955, Aug. 2009.
[31] L. Liu, S. Ding, and X. Yu, "Second-order sliding mode control design subject to an asymmetric output constraint," *IEEE Trans. Circuits Syst. II, Exp. Briefs*, vol. 68, no. 4, pp. 1278–1282, Apr. 2021.
[32] L. Liu and S. Ding, "A unified control approach to finite-time stabilization of SOSM dynamics subject to an output constraint," *Appl. Math. Comput.*, vol. 394, Apr. 2021, Art. no. 125752.
[33] L. Liu, W. X. Zheng, and S. Ding, "High-order sliding mode controller design subject to lower-triangular nonlinearity and its application to robotic system," *J. Franklin Inst.*, vol. 357, no. 15, pp. 10367–10386, Oct. 2020.
[34] L. Liu, W. X. Zheng, and S. Ding, "An adaptive SOSM controller design by using a sliding-mode-based filter and its application to buck converter," *IEEE Trans. Circuits Syst. I, Reg. Papers*, vol. 67, no. 7, pp. 2409–2418, Jul. 2020.
[35] S. Ding, J. H. Park, and C.-C. Chen, "Second-order sliding mode controller design with output constraint," *Automatica*, vol. 112, Feb. 2020, Art. no. 108704.
[36] W. Gao and J. C. Hung, "Variable structure control of nonlinear systems: A new approach," *IEEE Trans. Ind. Electron.*, vol. 40, no. 1, pp. 45–55, Feb. 1993.
[37] C. J. Fallaha, M. Saad, H. Y. Kanaan, and K. Al-Haddad, "Sliding-mode robot control with exponential reaching law," *IEEE Trans. Ind. Electron.*, vol. 58, no. 2, pp. 600–610, Feb. 2011.
[38] S. M. Mozayan, M. Saad, H. Vahedi, H. Fortin-Blanchette, and M. Soltani, "Sliding mode control of PMSG wind turbine based on enhanced exponential reaching law," *IEEE Trans. Ind. Electron.*, vol. 63, no. 10, pp. 6148–6159, Oct. 2016.
[39] K. B. Devika and S. Thomas, "Power rate exponential reaching law for enhanced performance of sliding mode control," *Int. J. Control Autom. Syst.*, vol. 15, pp. 2636–2645, Apr. 2017.
[40] G. Rohith, "Fractional power rate reaching law for augmented sliding mode performance," *J. Franklin Inst.*, vol. 358, no. 1, pp. 856–876, Jan. 2021.
[41] J. R. García-Sánchez, S. Tavera-Mosqueda, R. Silva-Ortigoza, V. M. Hernández-Guzmán, J. Sandoval-Gutiérrez, M. Marcelino-Aranda, H. Taud, and M. Marciano-Melchor, "Robust switched tracking control for wheeled mobile robots considering the actuators and drivers," *Sensors*, vol. 18, no. 12, p. 4316, 2018.
[42] X. Che, D. Tian, P. Jia, Y. Gao, and Y. Ren, "Terminal sliding mode control with a novel reaching law and sliding mode disturbance observer for inertial stabilization imaging sensor," *Sensors*, vol. 20, no. 11, p. 3107, May 2020.
[43] M. Cui, W. Liu, H. Liu, H. Jiang, and Z. Wang, "Extended state observer-based adaptive sliding mode control of differential-driving mobile robot with uncertainties," *Nonlinear Dyn.*, vol. 83, nos. 1–2, pp. 667–683, Jan. 2016.

LEPENG SONG (Fellow, IEEE) was born in Sigouyuan, Yao, Tongchuan, Shaanxi, China, in 1976. He received the B.S. degree in automation from Beijing Technology and Business University, Beijing, in 1999, and the M.S. degree in electrical engineering from Chongqing University, Chongqing, in 2010.

He is currently a Professor with the Chongqing University of Science and Technology. His research interests include agricultural automation, image processing, intelligent control, and optimization. He was a recipient the Second Prize of Science and Technology Progress of Chongqing, the Second Prize of Science and Technology Progress of China Non-ferrous Metals Industry Association, the Third Prize of Teaching Achievement of Chongqing, the Third Prize of Excellent Popular Science Works of Chongqing, and the Third Prize of Excellent Paper of Chongqing Education Science Research Institute.

JINPEN HUANG was born in Chongqing, China, in 1997. He is currently pursuing the master's degree with the Chongqing University of Science and Technology. His current research interest includes mobile robot modeling and control and control system optimization.

QIN LIANG was born in Chongqing, China, in 1997. She is currently pursuing the master's degree with the Chongqing University of Science and Technology. Her current research interest includes digital image processing and defect detection.

XIANWEN LIANG was born in Sichuan, China, in 1995. She is currently pursuing the master's degree with the Chongqing University of Science and Technology. Her current research interest includes computer vision, object detection, and machine learning.

LING NIE was born in Banan, Chongqing, China, in 1976. She received the B.S. degree in application of electronic technology from the China University of Petroleum, Dongying, China, in 1999, and the M.S. degree in instrument science and technology from Chongqing University, Chongqing, in 2005.

She is currently a Teacher with the Chongqing University of Science and Technology. Her research interests include automatic detection technology machinery and electronics. She was a recipient the First Prize of Petroleum Engineering Construction Science and Technology and the Third Prize of China Instrument Science and Technology.

JIANQU ZHU was born in Jiulongpo, Chongqing, China, in 1973. He received the M.S. degree in power electronics and drives from Xihua University, China, in 2005, and the Ph.D. degree in electrical system control and information technology from Southwest Jiaotong University, China, in 2021. He is currently an Associate Professor with the Chongqing University of Science and Technology. His current research interests include agricultural automation, intelligent control, and optimization.